第 35 卷第 7 期
2019 年 7 月

无 机 化 学 学 报
CHINESE JOURNAL OF INORGANIC CHEMISTRY

Vol.35 No.7
1121-1129

无模板法合成介孔棒状钴酸锰及其苯乙烯环氧化反应性能

徐 蔓 苏 航 邵 波 王 芸 周诗健* 孔 岩*
(南京工业大学化工学院,材料化学工程国家重点实验室,南京 211800)

摘要: 通过简单的无模板水热法及煅烧处理成功合成了介孔棒状钴酸锰。采用 X 射线衍射(XRD)、场发射扫描电镜(FE-SEM)、透射电镜(TEM)、氮气吸附-脱附和 X 射线光电子能谱(XPS)等手段对材料的晶体结构、表面形貌、孔结构和表面化学组成进行了表征。结果表明,目标产物钴酸锰样品介孔结构形成良好,孔径分布在 6 nm。此外,钴酸锰的棒状形貌直径为 100~200 nm,长度为 2~3 μm。相比于其他 Co 基、Mn 基催化剂,钴酸锰被首次应用在苯乙烯环氧化反应中,表现出了极高的催化活性,苯乙烯的转化率达到 95.8%,对氧化苯乙烯的选择性为 58.2%。而且,在 5 次循环试验后,催化活性并没有发生明显的改变,进一步证明了催化剂的稳定性。同时,系统研究了主要反应参数(反应时间、反应温度、苯乙烯/叔丁基过氧化氢(TBHP)的物质的量比值)对介孔棒状钴酸锰催化活性的影响。

关键词: 钴酸锰; 棒状形貌; 水热合成; 介孔结构; 环氧化
中图分类号: O643.32+2 **文献标识码**: A **文章编号**: 1001-4861(2019)07-1121-09
DOI:10.11862/CJIC.2019.155

Template-Free Synthesis and Boosting Catalytic Activity in Styrene Epoxidation of Mesoporous Rod-like $MnCo_2O_4$

XU Man SU Hang SHAO Bo WANG Yun ZHOU Shi-Jian* KONG Yan*
(*State Key Laboratory of Materials-Oriented Chemical Engineering, College of Chemical Engineering, Nanjing Tech University, Nanjing* 211800, *China*)

Abstract: Mesoporous rod-like $MnCo_2O_4$ was fabricated via a facile template-free hydrothermal method and subsequent calcination. The crystal structure, surface morphology, pore structure and surface chemical composition were characterized by X-ray diffraction (XRD), field emission scanning electron microscopy (FE-SEM), transmission electron microscopy (TEM), N_2 adsorption-desorption and X-ray photoelectron spectra (XPS). Characterization results revealed that, in the target $MnCo_2O_4$ sample, the mesoporous structure was well-formed, and the pore size distribution was defined in 6 nm. Also, the particular rod-like morphology was obtained in $MnCo_2O_4$ with diameters of 100~200 nm and a length of 2~3 μm. Based on these, the $MnCo_2O_4$ sample was firstly used as a heterogeneous catalyst in the epoxidation of styrene. Compared with other Co-based and Mn-based catalysts, it exhibited relatively high catalytic activity, the conversion rate of styrene was 95.8%, and the selectivity of styrene oxide was 58.2%. Moreover, after five cycles, the catalytic activity did not change significantly, further confirming the stability of $MnCo_2O_4$. Meanwhile, the effects of main reaction parameters (reaction time, reaction temperature, the molar ratio of styrene to *tert*-butyl hydroperoxide (TBHP)) on the catalytic activity of mesoporous rod-like $MnCo_2O_4$ were systematically investigated.

Keywords: $MnCo_2O_4$; rod-like morphology; hydrothermal synthesis; mesoporous structure; epoxidation

收稿日期:2019-02-21。收修改稿日期:2019-05-07。
国家自然科学基金(No.21476108,21276125,21776129,21706121)、江苏省自然科学基金(No.BK20170995)、江苏省高校自然科学研究项目(No.16KJB530003)和江苏省高等教育机构重点学科建设项目(PAPD)资助。
*通信联系人。E-mail:kongy36@njtech.edu.cn,zshijian@njtech.edu.cn

0 Introduction

Styrene oxide is an important intermediate for the formation of various products such as styrene glycol, surface coating, and cosmetics and so on[1-3]. Traditionally, it could be obtained by catalytic epoxidation of styrene with oxidants. It is well known that the type of oxidant in the styrene oxidation reaction has a great influence on the selectivity of the epoxidation products[4]. According to literature reports, it is evident that *tert*-butyl hydroperoxide (TBHP) is one of the most widely used oxidants in olefin epoxidation because of its low cost and high selectivity to epoxy compound[5]. So far, various kinds of catalysts, such as CeO_2[6], Mn_3O_4[1], NiO[7] and $Ce_xCo_{1-x}Fe_2O_4$[5] have been used in the styrene epoxidation due to their low cost and earth abundance. However, there are many problems in this series of catalysts, such as low styrene conversion rate, poor selectivity to styrene oxide, poor stability and difficulty in separation. Therefore, it is of great importance to explore novel catalysts with strong stability, excellent styrene conversion and high selectivity to styrene oxide.

Recently, cobalt oxide (Co_3O_4) is widely used in environmental chemistry and catalytic materials due to their stable chemical properties and good catalytic properties[8]. However, the toxicity and high cost of cobalt oxide limit its application in some aspects. Therefore, it is meaningful to partial substitution of Co in Co_3O_4 with Mn to reduce the amount of toxic Co (cobalt manganese ternary oxides, $Co_xMn_{3-x}O_4$, x=1, 2) because manganese is cheap, rich in nature and chemically stable[9]. In addition, the complex chemical composition and synergistic effects between Co and Mn also lead to excellent catalytic activity[10]. Therefore, the bimetallic cobalt-manganese oxide ($MnCo_2O_4$) has been extensively studied by researchers. As we know, apart from the composition, the morphology and pore structure could also affect the catalytic performance to some extent[11]. In particular, the special morphology may provide more exposed active sites and affect the external diffusion effect, while the mesoporous channels may promote the transport/diffusion of the reactant and product molecules during the heterogeneous catalytic reaction process[12]. So far, the $MnCo_2O_4$ catalysts with different morphologies and structures, such as multiporous microspheres[13], microbars[14] and 3D nanosphere[15] have been synthesized via different methods. And the general method for synthesizing mesoporous $MnCo_2O_4$ was template-assisted method[16]. However, the removal of templating agents during the synthesis process leads to more complicated operations and high cost. Therefore, it is necessary to synthesize $MnCo_2O_4$ catalysts with special morphology and better pore structure via a facile method. Moreover, to the best of our knowledge, the $MnCo_2O_4$ catalysts with rod-like morphology are rarely reported, and as a heterogeneous catalyst, it is seldom used in the styrene epoxidation reaction.

Herein, we report a facile template-free hydrothermal method to synthesize the mesoporous rod-like $MnCo_2O_4$ with a defined pore size distribution, and styrene epoxidation reaction was selected as the target reaction to assess the catalytic performance of mesoporous rod-like $MnCo_2O_4$.

1 Experimental

1.1 Materials

In this experiment, cobalt nitrate hexahydrate ($Co(NO_3)_2\cdot 6H_2O$, analytical grade) and hexamethylenetetramine (HMT) were purchased from West Long Chemical Co., Ltd. Manganese nitrate tetrahydrate ($Mn(NO_3)_2\cdot 4H_2O$, analytical grade) was purchased from Sinopharm Group Chemical Reagent Co., Ltd. Ammonium fluoride (NH_4F) was purchased from Nanjing Chemical Reagent Co., Ltd. *tert*-butyl hydroperoxide (TBHP), acetonitrile and styrene were purchased from Sinopharm Chemical Reagent Co., Ltd. All chemicals were used as received without further purification.

1.2 Synthesis of $MnCo_2O_4$

In a typical synthesis, 2 mmol $Co(NO_3)_2\cdot 6H_2O$, 1 mmol $Mn(NO_3)_2\cdot 4H_2O$, 20 mmol HMT, 15 mmol NH_4F were dissolved in 30 mL deionized water under magnetic stirring. Then, the homogeneous solution was transferred into a Teflon-lined stainless steel autoclave, and heated at 120 ℃ for 6 h. The obtained pink powders were washed with deionized water and ethyl alcohol three times, respectively. Then the sample was dried at 60 ℃ for 24 h. Finally the precursor was calcined at 600 ℃ for 4 h to obtain the final product $MnCo_2O_4$. For comparison, the Co_3O_4 and MnO_x were synthesized under similar conditions, except that $Mn(NO_3)_2\cdot 4H_2O$ and $Co(NO_3)_2\cdot 6H_2O$ were absent in the reaction solution.

1.3 Characterizations

X-ray diffraction (XRD) patterns were recorded using a Smartlab TM 9 KW (Rigaku Corporation, Tokyo, Japan) equipped with a rotating anode and Cu $K\alpha$ radiation (λ=0.154 178 nm), and operated at 40 kV and 100 mA in a range of 10°~80°. The N_2 adsorption-desorption measurements were carried out in the relative pressure (P/P_0) range from 0.01 to 0.99 under (77.4 K), and the specific surface areas and distribution of pore size were calculated using the Brunauer-Emmet-Teller (BET) and Barrett-Joyner-Halenda (BJH) methods, respectively. Field emission scanning electron microscopy (FE-SEM) was performed on a Hitachi S4800 Field Emission Scanning Electron Microscopy and operated at 5 kV and 10 μA. Transmission electron microscopy (TEM) images were recorded on a JEM-2010 EX microscope with the accelerating voltage at 200 kV. Hydrogen temperature programmed reduction (H_2-TPR) measurements were performed utilizing a fixed-bed reactor under a flow of 10%(V/V) H_2/Ar gas mixture and a heating rate of 10 ℃·min^{-1} from room temperature to 700 ℃. Before the TPR analysis, the carbonates and hydrates impurities were removed by flowing argon over the catalyst at a flow rate of 30 mL·min^{-1} at 300 ℃ for 1 h, then cooled to room temperature. The X-ray photoelectron spectra (XPS) were measured on a PHI 5000 Versa Probe X-ray photoelectron spectrometer (Thermo Scientific Escalab 250Xi) equipped with Al $K\alpha$ radiation (1 486.6 eV). The C1*s* peak at 284.8 eV was used as the reference for binding energies.

1.4 Catalysis tests

The catalytic reaction was carried out in a 25 mL three-necked round bottom flask fitted with a reflux condenser. Typically, 10 mL acetonitrile, 1 mmol styrene, and 10 mg catalyst were mixed within the flask. Then, 3 mmol TBHP was added to the mixture solution under stirring. The reaction was maintained at 80 ℃ for 10 h. The catalytic conversion rate of styrene and selectivity were determined using GC-3900 gas chromatograph.

2 Results and discussion

2.1 Crystal structure

Fig.1 shows the XRD pattern of the sample, all the diffraction peaks could be indexed to the $MnCo_2O_4$ (PDF No.23-1237) with spinel structure, the peaks at *ca.* 18.5°, 30.5°, 36°, 37.6°, 43.8°, 54.3°, 58°, and 63.6° can be ascribed to the (111), (220), (311), (222), (400), (422), (511), and (440) crystal planes, respectively. Meanwhile, there was no other impurity diffraction peak appeared, indicating the high purity of the as-prepared sample.

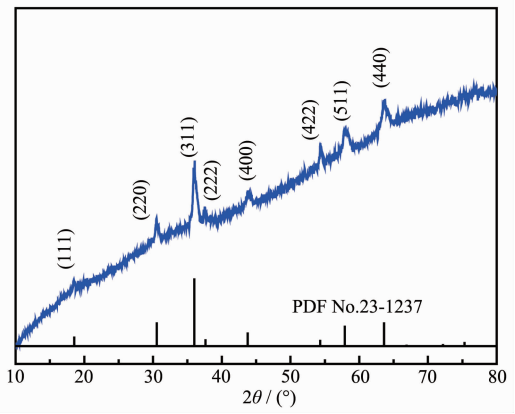


Fig.1　XRD pattern of the sample

2.2 Surface morphology

The morphology of the obtained sample was investigated by SEM and TEM techniques. As shown in Fig.2a, the precursor exhibit significant rod-like morphology with the diameter of 100~200 nm while the length was up to 2~3 μm. It can be seen from Fig.2b, after calcination, this rod-like morphology was still maintained in the final product of $MnCo_2O_4$, only with much rougher surface. This phenomenon could be due to the gas and steam released from the rod-like precursor during the heat treatment process, which made a lot of mesopores appear. This is further verified from the high resolution TEM (HR-TEM) result in Fig.2c, it can be clearly seen that the rod structure was composed of many nanoparticles with diameters of 6~14 nm. In Fig. 2d, the lattice fringe spacing of 0.25 and 0.15 nm corresponded to the (311) and (440) planes of $MnCo_2O_4$, respectively. As shown in Fig.2(f~h), the elemental mapping images demonstrate that the Co, Mn, O were uniformly dispersed throughout the mesoporous rod-like $MnCo_2O_4$ structure.

2.3 Formation mechanism

It is necessary to give a reasonable explanation for the roles of HMT and NH_4F in the formation of mesoporous rod-like $MnCo_2O_4$. HMT is used as a precipitant,

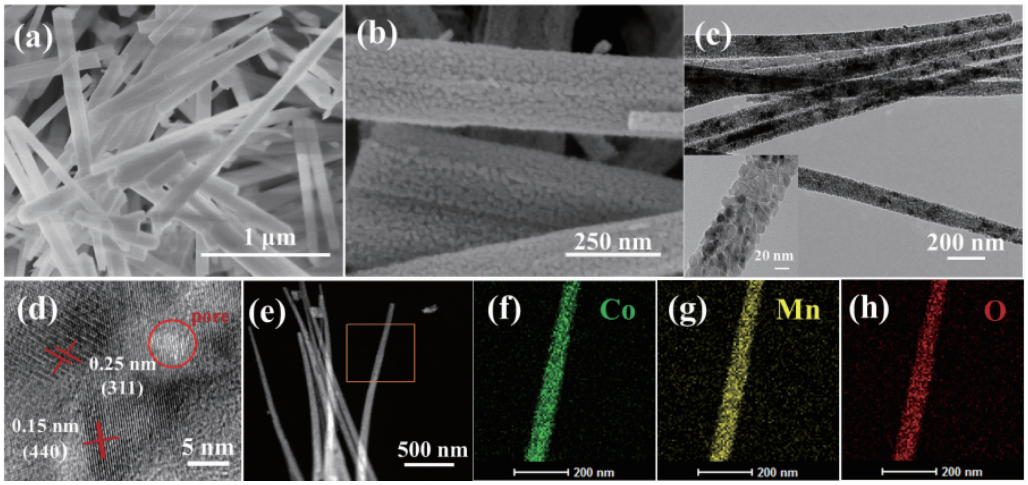
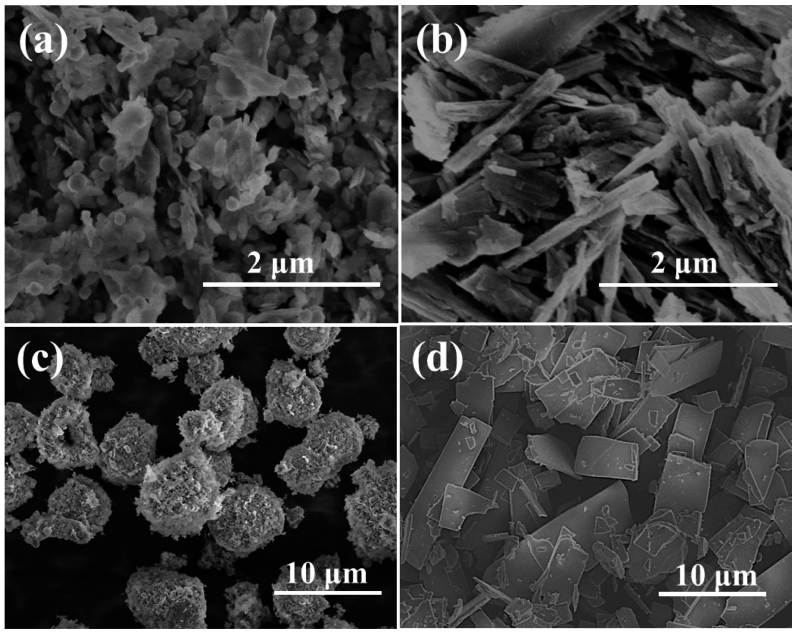


Fig.2 SEM images of (a) precursor and (b) final product $MnCo_2O_4$; (c, d) TEM and HR-TEM images of mesoporous rod-like $MnCo_2O_4$; (f~h) Elemental mapping of Co, Mn, and O of mesoporous rod-like $MnCo_2O_4$ in (e)

which can decompose to produce ammonia at temperatures above 70 ℃, and ammonia dissolves in water to produce OH^-. In the early stage of hydrothermal, the nucleation rate of the particles is slow, with the increase of hydrothermal time, the particles tend to form rod-like morphology through an anisotropic growth process [17]. However, we can see from Fig.3(a,b), when HMT was replaced with ammonia and NaOH, no rod-like structure was formed. Since ammonia or NaOH was rapidly hydrolyze to form OH^- when added to the solution, and the metal ions Co^{2+} and Mn^{2+} reacted with OH^- immediately to form metal hydroxide precursor. In this process, the nucleation rate of particles was very fast. Thus, other morphology of precursors are formed instead of rod-like structure[18-19]. Wang et al.[20] reported that the F^- with small radius may promote the formation of α-MnO_2 nanowires via a rolling process. In order to confirm the role of F^-, we replaced F^- with SO_4^{2-} and PO_4^{3-} while keeping other conditions unchanged. As shown in Fig.3 (c,d), we only got some urchin-like and plate-like structure instead of rod-like structure. This phenomenon can be ascribed to that the SO_4^{2-} and PO_4^{3-} anions with



(a) 20 mmol $NH_3 \cdot H_2O$, (b) 20 mmol NaOH, (c) 7.5 mmol $(NH_4)_2SO_4$ and (d) 5 mmol $(NH_4)_3PO_4 \cdot 3H_2O$

Fig.3 SEM images of Co-Mn hydroxide precursors at different conditions

larger radius, which may prevent or slow down the rolling process[21-22]. Based on these, a possible mechanism is proposed as follows: During the hydrothermal process, HMT is gradually decomposed into formaldehyde and ammonia, and the ammonia is reacted with H_2O to produce OH^-. Then, these produced OH^- reacts with Co^{2+} and Mn^{2+} to form Co-Mn hydroxide nanoparticles under the hydrothermal condition[23]. At this stage, in order to reduce the surface energy, the irregular nanoparticles with high surface energy are randomly aggregated and self-assembling under van der Waals force and crystal surface attraction, leading to the formation of rod-like morphology[24]. Xia et al.[25] reported that the F^- has strong coordination ability, therefore, the Co^{2+} and Mn^{2+} also tend to coordinate with F^-. Therefore, we conclude that the presence of F^- may regulate the reaction rate and contribute to the formation of the final rod morphology via a rolling process[26-27]. Finally, the mesoporous rod-like $MnCo_2O_4$ was obtained after a calcination process, the formation of pore structure can be attributed to the release of the gas from the decomposition of rod-like precursors[28-29]. The formation process is shown in Fig.4.

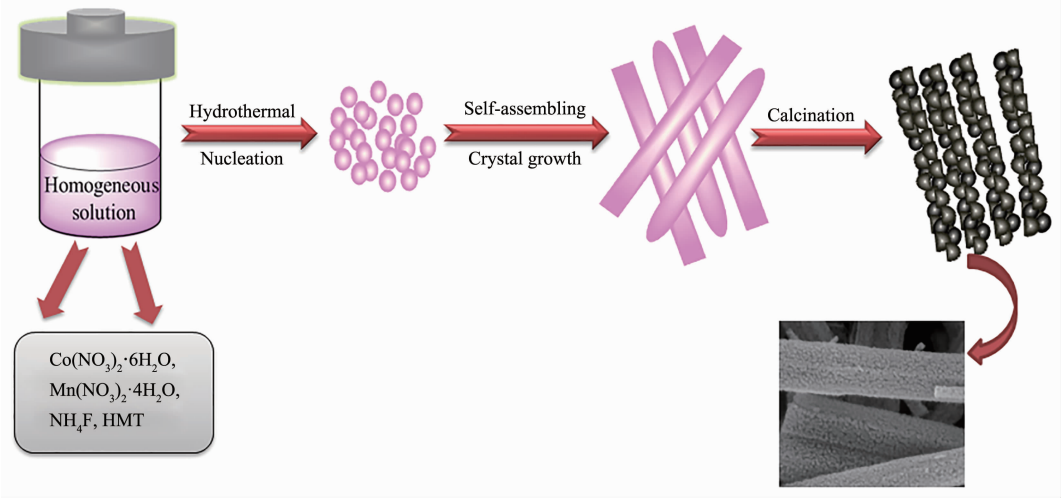


Fig.4　Schematic illustration of the preparation process of the mesoporous rod-like $MnCo_2O_4$

2.4　N_2 adsorption-desorption isotherm

The specific surface area and pore size distribution were measured by N_2 adsorption-desorption test. As shown in Fig.5, the curve of the rod-like $MnCo_2O_4$ displayed type-Ⅳ isotherm with H3 hysteresis loop, suggesting the existence of well-defined mesoporous structure. The specific surface area (S_{BET}) of $MnCo_2O_4$ was calculated to be 65 $m^2 \cdot g^{-1}$ and the pore size distribution (inset) exhibited one dominant peak centered at 6 nm, indicating the well-formed mesoporous structure with a defined pore size distribution in the target sample. This is consistent with the SEM and TEM results.

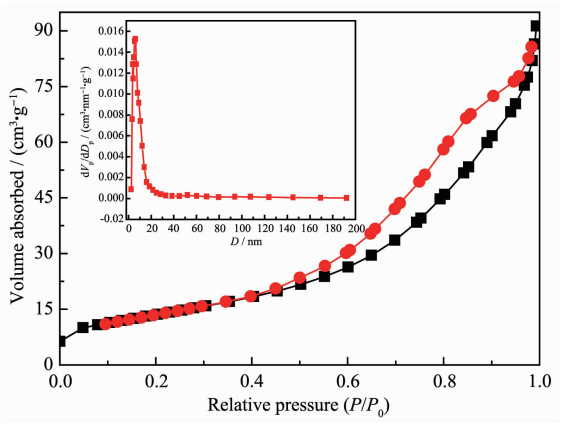


Fig.5　N_2 adsorption-desorption isotherm and pore size distribution curve of the meosporous rod-like $MnCo_2O_4$

2.5　XPS analysis

The composition and valence states of the as-synthesized mesoporous rod-like $MnCo_2O_4$ were studied by XPS. As shown in Fig.6a, the survey spectrum demonstrated the presence of Co, Mn, O and C, where the C derived from the reference. It can be clearly seen from Fig.6b, the two peaks located at 779.7 and 795.0 eV were the characteristic peaks of $Co2p_{3/2}$ and $Co2p_{1/2}$, respectively, and two obvious satellite peaks were observed, indicating the co-existence of Co^{2+} and Co^{3+} in mesoporous rod-like $MnCo_2O_4$. Moreover, the $Co2p$

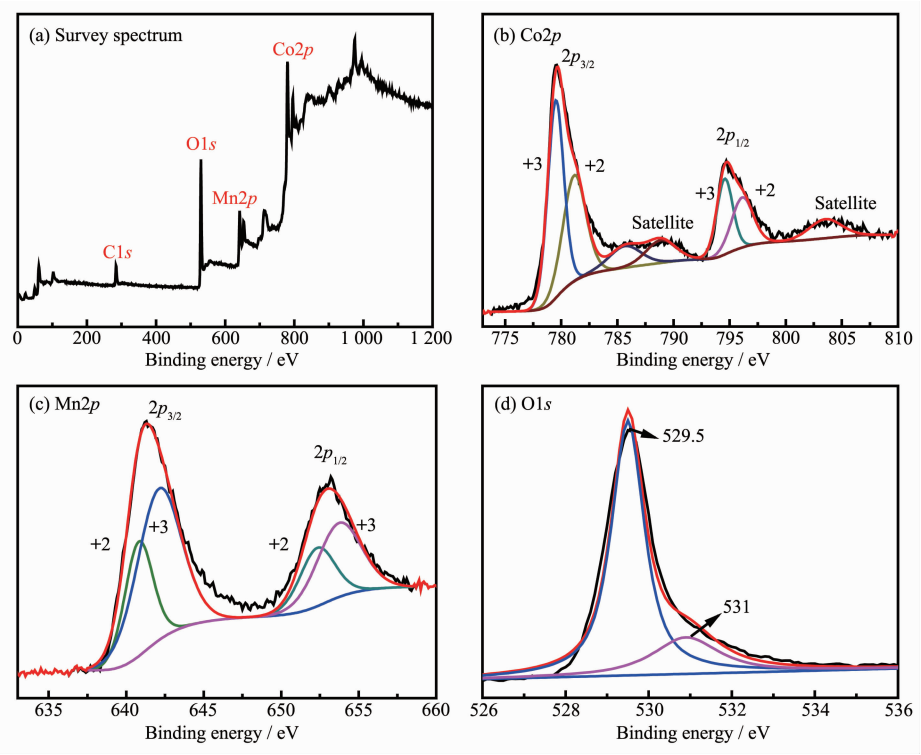


Fig.6 XPS spectra of the mesoporous rod-like $MnCo_2O_4$

spectrum was fitted well to two spin-orbit doublets characteristic of Co^{2+} and Co^{3+}, the peaks located at 781.2 and 796.1 eV were ascribed to the Co^{2+}, and the peaks at 779.5 and 794.6 eV were attribute to the Co^{3+} [30-31]. The Mn2*p* spectrum (Fig.6c) was divided into four peaks by using a Gaussian fitting method. The peaks at around 640.7 and 652.6 eV can be assigned to the Mn^{2+}, the other two peaks located at 642.8 and 654.2 eV can be ascribed to the Mn^{3+} [32]. Therefore, it can be concluded that Mn^{2+}/Mn^{3+} and Co^{2+}/Co^{3+} coexist in the mesoporous rod-like $MnCo_2O_4$, which is consistent with the literature reported[33-34]. Fig.6d shows the O1*s* spectrum, the peaks at around 529.5 and 531 eV could be attributed to the lattice oxygen and hydroxyl oxygen species, respectively[35].

2.6 H_2-TPR analysis

Normally, the catalytic activity of the redox reaction is mainly related with the reducibility of the metal active sites in the catalyst. Herein, the H_2-TPR experiments were carried out and the results are shown in Fig.7. In addition, two pristine samples of Co_3O_4 and MnO_x were prepared for comparison. As we can see, two reduction peaks at about 290 and 400 ℃ for Co_3O_4 could be ascribed to the stepwise reduction of $Co_3O_4 \rightarrow CoO \rightarrow Co$[8], while the peaks at about 336 and 439 ℃ observed in MnO_x were due to the transformation of $MnO_x \rightarrow Mn_3O_4 \rightarrow MnO$[16]. For mesoporous rod-like $MnCo_2O_4$, the peaks at about 331 and 438 ℃ were attributed to the stepwise reduction of $MnCo_2O_4$, whereas the peak at lower temperature (225 ℃) should be ascribed to the reduction of surface oxygen species. Moreover, it should be noted that a new peak at extremely high temperature (525 ℃) was appeared in the $MnCo_2O_4$ sample, therefore, it is inferred from this phenomenon that there was a strong interaction between manganese oxide and cobalt oxide in $MnCo_2O_4$, which would play a synergistic role to increase the catalytic activity[16,36].

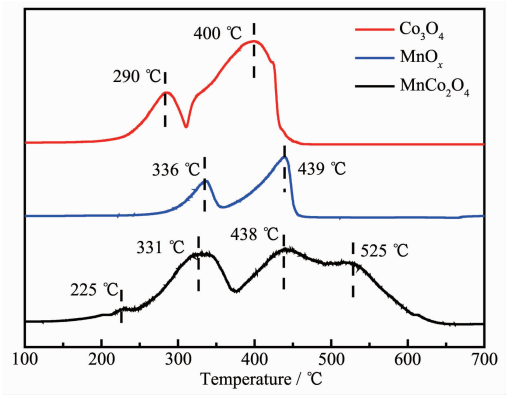


Fig.7 H_2-TPR profile of the samples

2.7 Catalytic performance

The catalytic activity of mesoporous rod-like $MnCo_2O_4$ was evaluated by catalyzing epoxidation of styrene. For comparison, the catalytic performance of hybrid MnO_2-Co_3O_4, Co-based and Mn-based catalysts are also listed in Table 1. It can be seen that, compared with MnO_2-Co_3O_4, mesoporous MnO_2 and mesoporous Co_3O_4 catalysts, the mesoporous rod-like $MnCo_2O_4$ showed extremely high catalytic performance, the conversion rate of styrene was 95.8%, and the selectivity of styrene oxide was 58.2%. This could be due to the large surface area in the mesoporous rod-like $MnCo_2O_4$, making more active sites exposed and available in the catalytic reaction. In addition, the mesoporous channels are also facilitate to the diffusion/transport of the reactant and product molecules during the catalytic reaction process. However, compared with the catalysts of Co-MCM-41 and Mn/SBA-15, the catalyst of the mesoporous rod-like $MnCo_2O_4$ showed much better catalytic properties, even with lower surface area. To explain this, it should be noted that there is a synergistic effect between Co and Mn species, in which the Co species play as the main active sites, and Mn species are mainly responsible for promoting the transfer of electrons during the reaction process because of their high conductivity[37]. Based on these, the catalyst of mesoporous rod-like $MnCo_2O_4$ could be chosen as the best candidate for the epoxidation of styrene.

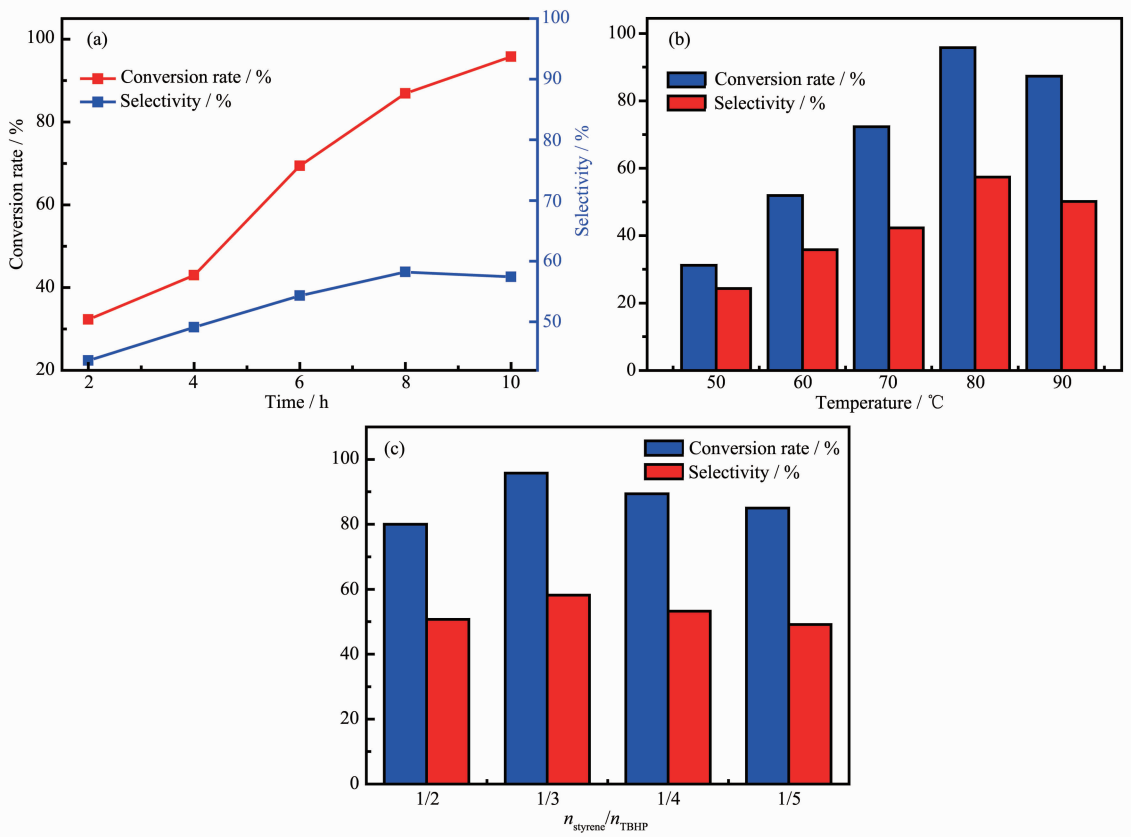
It is well known that the reaction conditions have a great influence on the conversion rate of styrene and the selectivity of styrene oxide. Therefore, the main reaction parameters, such as reaction time, reaction temperature and molar radio of styrene to TBHP were investigated. It can be clearly seen from Fig.8a, with the extension of time, the styrene conversion rate and the selectivity to styrene oxide were increased. Upon to 10 h, the styrene conversion was reached to 95.8%, however, there was a slight decrease in the selectivity for styrene oxide compared with 8 h. This phenomenon could be ascribed to the over-oxidation and hydrolysis of styrene oxide to form other by-products. As shown in Fig.8b, when the temperature of the catalytic reaction increased, the conversion rate of styrene and the selectivity of styrene oxide were increased, and the best catalytic performance was achieved at the temperature of 80 ℃. This can be attributed to the high temperature causing an increase in the collision of the reactants with the catalyst, thus an increase in the conversion rate of styrene was observed. However, further increasing the reaction temperature may result in decomposition of the oxidant TBHP and decreased the conversion rate. As shown in Fig.8c, the conversion rate of styrene and the selectivity to styrene oxide increased gradually as the molar ratio of styrene to TBHP decreased from 1/2 to 1/3. However, when the molar ratio of styrene to TBHP continued to decreased, the conversion rate and selectivity to styrene oxide decreased. This demonstrates that low concentration of TBHP caused a slow reaction while high TBHP concentration may compete with the styrene to occupy the active sites on the catalyst surface and slow down the reaction. Therefore, the optimal reaction conditions were as follows: reaction time of 10 h, reaction temperature of 80 ℃, and styrene/TBHP ratio of 1:3.

A series of experiments were conducted under the same conditions to evaluate the stability of the mesoporous rod-like $MnCo_2O_4$. As shown in Fig.9a, the mesoporous rod-like $MnCo_2O_4$ still exhibited high conversion rate and selectivity after five successive

Table 1　Catalytic performance of different samples in the epoxidation of styrene

Sample	S_{BET} / ($m^2 \cdot g^{-1}$)	Oxidant	Temperature / ℃	Conversion rate / %	Selectivity (SO^a) / %	Yield of SO / %	Reference
Mesoporous rod-like $MnCo_2O_4$	65	TBHP	80	95.8	58.2	55.8	This work
MnO_2-Co_3O_4	18	TBHP	80	19.3	28.1	5.4	[38]
Mesoporous MnO_2	27	TBHP	80	78.3	25.1	19.7	[38]
Mesoporous Co_3O_4 sheets	11.7	TBHP	80	53.4	62.2	33.2	[39]
Co-MCM-41	1 143	TBHP	100	79	6.9	5.5	[40]
Mn/SBA-15	157	TBHP	80	90	26	23.4	[41]

Reaction conditions: 10 mL acetonitrile, 1 mmol styrene, 10 mg catalyst, 3 mmol TBHP, 80 ℃, 10 h, reflux; [a]SO: styrene oxide.



Reaction conditions: (a) 10 mL acetonitrile, 1 mmol styrene, 10 mg catalyst, 3 mmol TBHP, 80 ℃; (b) 10 mL acetonitrile, 1 mmol styrene, 10 mg catalyst, 3 mmol TBHP, 10 h; (c) 10 mL acetonitrile, 1 mmol styrene, 10 mg catalyst, 80 ℃, 10 h

Fig.8 Effects of (a) reaction time, (b) reaction temperature and (c) molar ratio of styrene to TBHP on the catalytic performance of the mesoporous rod-like $MnCo_2O_4$

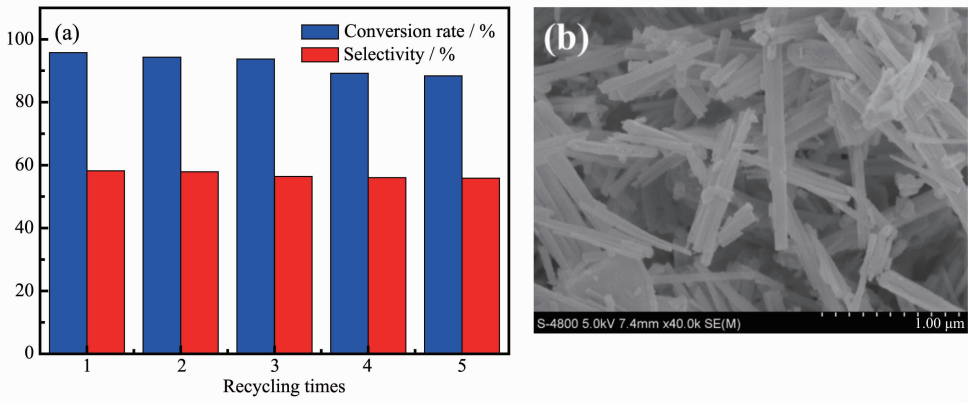


Fig.9 (a) Stability test of the $MnCo_2O_4$ catalyst and (b) SEM images of $MnCo_2O_4$ catalyst after the recycling experiments

recycle tests, and the reused sample also displayed the typical rod morphology (Fig.9b), verifying the high reusability and potential practical application ability.

3 Conclusions

In summary, the rod-like $MnCo_2O_4$ with mesoporous structure was successfully synthesized via a facile template-free hydrothermal method and subsequent calcination process. Such rod-like structure was composed of many nanoparticles with diameters of 6~14 nm. The target mesoporous rod-like $MnCo_2O_4$ sample showed higher surface area and better pore size distribution. In addition, it exhibited excellent catalytic activity and cycling performance in the styrene epoxidation reaction. We conclude that the superior catalytic performance can be ascribed to the synergistic

effects between Co species and Mn species of $MnCo_2O_4$ and the mesoporous structures. We believe that the facile strategy can be extended to synthesize other mesoporous spinel-type binary metal oxides (AB_2O_4) with excellent catalytic performance. In addition, the mesoporous rod-like $MnCo_2O_4$ could be chosen as the best candidate for the epoxidation of styrene.

References:

[1] Askarinejad A, Bagherzadeh M, Morsali A. *Appl. Surf. Sci.*, **2010**,**256**(22):6678-6682

[2] Liu J Y, Chen T T, Jian P M, et al. *J. Colloid Interface Sci.*, **2018**,**526**:295-301

[3] Masunga N, Doyle B P, Carleschi E, et al. *Appl. Catal. A*, **2018**,**559**:175-186

[4] Yang F, Zhou S J, Gao S Y, et al. *Microporous Mesoporous Mater.*, **2017**,**238**:69-77

[5] Tong J H, Li W Y, Bo L L, et al. *J. Catal.*, **2016**,**344**:474-481

[6] Pal P, Pahari S K, Sinhamahapatra A, et al. *RSC Adv.*, **2013**, **3**(27):10837-10847

[7] Choudhary V R, Jha R, Jana P. *Catal. Commun.*, **2008**,**10**(2): 205-207

[8] Teng F, Chen M D, Li G Q, et al. *Appl. Catal. B*, **2011**,**110**: 133-140

[9] Yao Y J, Cai Y M, Wu G D, et al. *J. Hazard. Mater.*, **2015**, **296**:128-137

[10]Yang F, Ding Y, Tang J J, et al. *Mol. Catal.*, **2017**,**435**:144-155

[11]Wang H Q, Gao S Y, Du J, et al. *Appl. Catal. A*, **2015**,**504**: 228-237

[12]Liu P, Hao Q L, Xia X F, et al. *J. Phys. Chem. C*, **2015**,**119** (16):8537-8546

[13]Ma S C, Sun L Q, Cong L N, et al. *J. Phys. Chem. C*, **2013**, **117**:25890-25897

[14]Wang L J, Liu B, Ran S H, et al. *J. Mater. Chem. A*, **2013**, **1**:2139-2143

[15]Hu X N, Huang L, Zhang J P, et al. *J. Mater. Chem. A*, **2018**,**6**(7):2952-2963

[16]Qiu M Y, Zhan S H, Yu H B, et al. *Nanoscale*, **2015**,**7**(6): 2568-2577

[17]Hu X L, Huang H H, Zhang J B, et al. *RSC Adv.*, **2015**,**5**: 99899-99906

[18]Zhang Y Q, Li L, Shi S J, et al. *J. Power Sources*, **2014**,**256**: 200-205

[19]Jia B R, Qin M L, Li S M, et al. *ACS Appl. Mater. Interfaces*, **2016**,**8**:15582-15590

[20]Wang X H, Ni S B, Zhou G, et al. *Mater. Lett.*, **2010**,**64**(13): 1496-1498

[21]Gao Y Q, Wang Z H, Wan J X, et al. *J. Cryst. Growth*, **2005**, **279**:415-419

[22]Wang X, Li Y D. *Chem. Eur. J.*, **2003**,**9**(1):300-306

[23]Liu T, Liu J Y, Liu Q, et al. *Nanoscale*, **2015**,**7**(46):19714-19721

[24]Liu T, Liu J Y, Liu Q, et al. *Sens. Actuators B*, **2017**,**250**: 111-120

[25]Xia X H, Tu J P, Zhang Y Q, et al. *ACS Nano.*, **2012**,**6**: 5531-5538

[26]Liu S M, Zhang W Q, Chen N, et al. *ChemElectroChem*, **2018**,**5**(16):2181-2185

[27]Long H W, Liu T M, Zeng W, et al. *Mater. Lett.*, **2018**,**214**: 127-129

[28]Shu Z, Huang W M, Hua Z L, et al. *J. Mater. Chem. A*, **2013**,**1**(35):10218-10227

[29]Zhang G J, Shen Z R, Liu M, et al. *J. Phys. Chem. B*, **2006**, **110**:25782-25790

[30]Liao F, Han X R, Zhang Y F, et al. *Ceram. Int.*, **2018**,**44**: 22622-22631

[31]Li G D, Xu L Q, Zhai Y J, et al. *J. Mater. Chem. A*, **2015**,**3**: 14298-14306

[32]Kong X Z, Zhu T, Cheng F Y, et al. *ACS Appl. Mater. Interfaces*, **2018**,**10**(10):8730-8738

[33]Xu J S, Sun Y D J, Lu M, et al. *Acta Mater.*, **2018**,**152**:162-174

[34]FENG Yan(冯艳), WU Jian-Bo(吴剑波), ZHANG Xiao-Ling (张晓玲), et al. *Chinese J. Inorg. Chem.*(无机化学学报), **2019**,**35**(4):569-579

[35]Yao L L, Zhang L L, Liu Y X, et al. *CrystEngComm*, **2016**, **18**:8887-8897

[36]Wang Y, Guo L M, Chen M Q, et al. *Catal. Sci. Technol.*, **2018**,**8**(2):459-471

[37]Kuang L P, Ji F Z, Pan X X, et al. *Chem. Eng. J.*, **2017**, **315**:491-499

[38]Masunga N, Tito G S, Meijboom R. *Appl. Catal. A*, **2018**, **552**:154-167

[39]Liu J Y, Chen T T, Yan X D, et al. *Catal. Commun.*, **2018**, **109**:71-75

[40]Tang Q H, Zhang Q H, Wu H L, et al. *J. Catal.*, **2005**,**230** (2):384-397

[41]Sweta V C. *Chin. J. Chem. Eng.*, **2018**,**26**(6):1300-1306